Endocrinology, 2023, **164**, 1–15
https://doi.org/10.1210/endocr/bqad028
Advance access publication 12 February 2023
Research Article

Enhanced Endosomal Signaling and Desensitization of GLP-1R vs GIPR in Pancreatic Beta Cells

Yusman Manchanda,[1] Stavroula Bitsi,[1] Shiqian Chen,[2] Johannes Broichhagen,[3] Jorge Bernardino de la Serna,[4] Ben Jones,[2,*] and Alejandra Tomas[1,*]

[1]Section of Cell Biology and Functional Genomics, Department of Metabolism, Digestion and Reproduction, Imperial College London, London W12 0NN, UK
[2]Section of Endocrinology and Investigative Medicine, Department of Metabolism, Digestion and Reproduction, Imperial College London, London W12 0NN, UK
[3]Chemical Biology, Leibniz-Forschungsinstitut für Molekulare Pharmakologie (FMP), Berlin 13125, Germany
[4]National Heart and Lung Institute, Imperial College London, London W12 0NN, UK

Correspondence: Alejandra Tomas, PhD, Section of Cell Biology and Functional Genomics, Division of Diabetes, Endocrinology and Metabolism, Department of Metabolism, Digestion and Reproduction, Imperial College London, Hammersmith Campus, Du Cane Road, London W12 0NN, UK, Email: a.tomas-catala@imperial.ac.uk; or Ben Jones, MD, PhD, Section of Endocrinology and Investigative Medicine, Division of Diabetes, Endocrinology and Metabolism, Department of Metabolism, Digestion and Reproduction, Imperial College London, Hammersmith Campus, Du Cane Road, London W12 0NN, UK, Email: ben.jones@imperial.ac.uk.
*Joint senior and corresponding authors.

Abstract

The incretin receptors, glucagon-like peptide-1 receptor (GLP-1R) and glucose-dependent insulinotropic polypeptide receptor (GIPR), are prime therapeutic targets for the treatment of type 2 diabetes (T2D) and obesity. They are expressed in pancreatic beta cells where they potentiate insulin release in response to food intake. Despite GIP being the main incretin in healthy individuals, GLP-1R has been favored as a therapeutic target due to blunted GIPR responses in T2D patients and conflicting effects of GIPR agonists and antagonists in improving glucose tolerance and preventing weight gain. There is, however, a recently renewed interest in GIPR biology, following the realization that GIPR responses can be restored after an initial period of blood glucose normalization and the recent development of dual GLP-1R/GIPR agonists with superior capacity for controlling blood glucose levels and weight. The importance of GLP-1R trafficking and subcellular signaling in the control of receptor outputs is well established, but little is known about the pattern of spatiotemporal signaling from the GIPR in beta cells. Here, we have directly compared surface expression, trafficking, and signaling characteristics of both incretin receptors in pancreatic beta cells to identify potential differences that might underlie distinct pharmacological responses associated with each receptor. Our results indicate increased cell surface levels, internalization, degradation, and endosomal vs plasma membrane activity for the GLP-1R, while the GIPR is instead associated with increased plasma membrane recycling, reduced desensitization, and enhanced downstream signal amplification. These differences might have potential implications for the capacity of each incretin receptor to control beta cell function.

Key Words: incretin, beta cell, GLP-1R, GIPR, trafficking, signal compartmentalization

Abbreviations: 2D, 2-dimensional; AUC, area under the curve; BSA, bovine serum albumin; DERET, diffusion-enhanced resonance energy transfer; FITC, fluorescein isothiocyanate; GIPR, glucose-dependent insulinotropic polypeptide receptor; GLP-1R, glucagon-like peptide 1 receptor; HTRF, homogeneous time-resolved fluorescence; KO, knockout; RICS, Raster image correlation spectroscopy; ROI, region of interest; T2D, type 2 diabetes; TMR, tetramethylrhodamine; TR-FRET, time-resolved fluorescence resonance energy transfer.

Incretin receptors, comprising the glucagon-like peptide-1 receptor (GLP-1R) and the glucose-dependent insulinotropic polypeptide receptor (GIPR), are key components of the glucoregulatory system due to their capacity to prevent postprandial hyperglycemia by amplifying insulin secretion from pancreatic beta cells in a glucose-dependent manner (1). Since their discovery and cloning in the 1990s (2-4), both receptors have been recognized for their glucose lowering potential. However, while the GLP-1R has successfully been exploited for the treatment of type 2 diabetes (T2D), with several pharmacological GLP-1R agonists currently in use clinically or undergoing clinical trials (5), the GIPR has not until recently been intensively pursued as a T2D treatment target, primarily due to GIP responses being blunted in T2D patients (6) and the perception that GIPR activation leads to weight gain, as inferred from the observation that GIPR knockout (KO) mice are protected against the effects of an obesogenic diet (7). As a result, antagonizing rather than activating the GIPR has been suggested as a potential therapeutic intervention for diabetes and obesity (8, 9). However, recent data from preclinical and clinical studies appear to contradict these assumptions regarding the role of GIPR in diabetes, as GIPR agonists have been shown to improve glucose tolerance and reduce body weight in T2D patients (10), and dual GLP-1R/GIPR targeting peptides, such as the recently developed tirzepatide, have demonstrated enhanced efficacy compared with currently approved GLP-1R agonist monotherapies (11).

Received: 5 December 2022. **Editorial Decision:** 6 February 2023. **Corrected and Typeset:** 15 March 2023

Previous studies from our group and others have demonstrated that changes in the spatiotemporal regulation of signaling play a crucial role in determining the metabolic outcomes of GLP-1R activation (12) and underlie the enhanced therapeutic effects of partial or biased GLP-1R agonists (13). However, neither the GIPR trafficking nor the spatiotemporal regulation of signaling by active GIPRs have been well characterized, despite the potential importance of these processes in the paradoxical responses obtained with both GIPR agonists and antagonists. GIPR has seldom been compared directly to GLP-1R in pancreatic beta cell systems, the primary cell type in which these related receptors coexist and exert many of their metabolic effects. In whole islets, both GLP-1R and GIPR stimulate insulin secretion in a glucose-dependent manner, but only GLP-1R retains its insulinotropic action in islets from diabetic models, implying that glucotoxicity specifically impairs GIP-dependent action in beta cells (14). However, the molecular mechanisms that explain the preservation of insulinotropic actions of GLP-1R but not GIPR in T2D remain unclear, with some suggestions that include reduced GIPR expression (15), increased GIPR degradation (16), and differences in $G\alpha_s$ vs $G\alpha_q$ coupling for each receptor (17). Of note, GLP-1R and GIPR potentiation of insulin secretion seems to have different dependency on K_{ATP} channels (18, 19), suggesting differences in downstream signaling between the 2 incretin receptors.

In the present study, we present a dataset describing the effects of GLP-1R vs GIPR activation on target downregulation and compartmentalization of intracellular signaling responses specifically in pancreatic beta cells, unveiling striking differences between the trafficking and signaling signatures from the 2 incretin receptors within their native environment. In particular, we demonstrate that the beta cell GIPR is a slow-internalizing, fast-recycling receptor compared with the GLP-1R. This trafficking pattern is accompanied by a reduced capacity for clustering, endosomal vs plasma membrane signaling, lysosomal targeting, and degradation of GIPR in response to agonist stimulation, as well as significantly reduced GIPR vs GLP-1R coupling to downstream effectors such as $G\alpha_s$, $G\alpha_q$, and β-arrestin 2. Paradoxically, however, and despite notably reduced surface levels of GIPR vs GLP-1R in primary islets from healthy mice, GIPR stimulation leads to similar or even enhanced signaling outputs, suggesting a greater degree of signal amplification and reduced desensitization associated with this incretin receptor under nondiabetic conditions.

Materials and Methods

Peptides

Native sequence peptides including GLP-1(7-36)NH_2 (referred to as GLP-1) and GIP(1-42) (referred to as GIP), and their fluorescein isothiocyanate (FITC) and tetramethylrhodamine (TMR) conjugates were obtained from Wuxi Apptec at >90% purity.

Cell Culture

Parental male rat insulinoma INS-1 832/3 cells (a gift from Prof. Christopher Newgard, Duke University, USA), INS-1 832/3 cells with endogenous GLP-1R or GIPR deleted by CRISPR/Cas9 (20) (a gift from Dr. Jacqueline Naylor, MedImmune), and corresponding multiclonal INS-1 832/3 cells stably expressing SNAP-GLP-1R or SNAP-GIPR (generated by transfecting GLP-1R KO or GIPR KO cells with SNAP-GLP-1R or SNAP-GIPR constructs (Cisbio), respectively, followed by selection with 1 mg/mL G418, FACS sorting of the population of SNAP-receptor-expressing cells and maintenance in 0.5 mg/mL G418) were cultured in RPMI-1640 with 11 mM D-glucose, supplemented with 10% FBS, 10 mM HEPES, 1 mM sodium pyruvate, 50 μM β-mercaptoethanol, and 1% penicillin/streptomycin in a 37 °C/5% CO_2 incubator.

Diffusion-Enhanced Resonance Energy Transfer Internalization Assays

The diffusion-enhanced resonance energy transfer (DERET) assay was performed as previously described (21). The INS-1 832/3 SNAP-GLP-1R or SNAP-GIPR cells were labeled in suspension with Lumi4-Tb (40 nM) for 30 minutes in complete media. After washing, cells were resuspended in HBSS containing 24 μM fluorescein and dispensed into 96-well white plates. A baseline read was serially recorded over 5 minutes using a Flexstation 3 instrument at 37 °C in time-resolved fluorescence resonance energy transfer (TR-FRET) mode using the following settings: λ_{ex} 340 nm, λ_{em} 520 and 620 nm, auto-cutoff, delay 400 μs, integration time 1500 μs. Ligands were then added, after which signal was repeatedly recorded for 30 minutes. Fluorescence signals were expressed ratiometrically after first subtracting signal from wells containing 24 μM fluorescein but no cells. Internalization was quantified as area under the curve (AUC) relative to individual well baseline.

High-content Microscopy Assays for Receptor Internalization and Recycling

The assay was performed as previously described (21). The INS-1 832/3 SNAP-GLP-1R or SNAP-GIPR cells were seeded into poly-D-lysine-coated, black 96-well plates. On the day of the assay, labeling was performed with BG-S-S-649 (1 μM), a surface-labeling SNAP-tag probe that can be released on application of reducing agents such as Mesna. After washing, treatments were applied for 30 minutes at 37 °C in complete medium. Ligand was removed and cells washed with cold HBSS and placed on ice for subsequent steps. Mesna (100 mM in alkaline TNE buffer, pH 8.6) or alkaline TNE buffer without Mesna was applied for 5 minutes, and then washed with HBSS. Cells were imaged by widefield microscopy, with both epifluorescence and transmitted phase contrast images acquired. On imaging completion, HBSS was removed and replaced with fresh complete medium, and receptor was allowed to recycle for 60 minutes at 37 °C, followed by a second Mesna application to remove any receptor that had recycled to the plasma membrane, with the plate re-imaged as above. Internalized receptor at each time point was determined from cell-containing regions as determined from the phase contrast image using PHANTAST (22) and used to determine internalization and recycling parameters as previously described (21).

NanoBiT Complementation and NanoBRET Assays

Mini-G protein/β-arrestin-2 recruitment NanoBiT assays

Here the SmBiT was cloned in frame at the C-terminus of the GLP-1R and the GIPR by substitution of the Tango sequence

on FLAG-tagged GLP-1R-Tango or GIPR-Tango (a gift from Prof. Bryan Roth, University of North Carolina, USA; Addgene plasmids #66291 and #66294), respectively. Mini-Gs, mini-Gq, and mini-Gi plasmids, tagged at the N-terminus with LgBiT, were a gift from Prof. Nevin Lambert, Medical College of Georgia, USA. For β-arrestin 2 recruitment assays, β-arrestin 2 fused at the N-terminus to LgBiT (LgBiT-β-arrestin 2; Promega, plasmid no. CS1603B118) was chosen as it has previously been used successfully with other class B GPCRs. The INS-1 832/3 GLP-1R KO and GIPR KO cells were seeded in 12-well plates and co-transfected with 0.5 μg each of GLP-1R-SmBiT or GIPR-SmBiT and either LgBiT-mini-Gs, -mini-Gq, -mini-Gi or -β-arrestin 2.

KRAS/Rab5 bystander NanoBRET assays

GLP-1R-NanoLuc was generated in house by polymerase chain reaction (PCR) cloning of the NanoLuciferase sequence from pcDNA3.1-ccdB-NanoLuc (a gift from Prof. Mikko Taipale; Addgene plasmid # 87067) onto the C-terminus end of the SNAP-GLP-1R vector (CisBio), followed by site-directed mutagenesis of the GLP-1R stop codon. GIPR-NanoLuc was subsequently cloned in house by exchanging the GLP-1R for the GIPR in the GLP-1R-NanoLuc construct. KRAS- and Rab5-Venus plasmids were a gift from Prof. Kevin Pfleger, University of Western Australia. The INS-1 832/3 GLP-1R KO and GIPR KO cells were seeded in 12-well plates and co-transfected with 0.2 μg KRAS-Venus and 0.1 μg GLP-1R- or GIPR-NanoLuc, respectively, or 0.5 μg Rab5-Venus and 0.1 μg GLP-1R- or GIPR-NanoLuc, respectively.

Mini-Gs-Venus recruitment NanoBRET assays

Mini-Gs-Venus was a gift from Prof. Nevin Lambert, Augusta University, USA. INS-1 832/3 GLP-1R KO or GIPR KO cells were seeded in 12-well plates and co-transfected with 0.5 μg mini-Gs-Venus and either 0.5 μg GLP-1R- or GIPR-NanoLuc, respectively.

Nb37 bystander NanoBiT assays

The Nb37 assay constructs were kindly provided by Prof. Asuka Inoue, Tohoku University, Japan. Nb37 (gene synthesized by GenScript with codon optimization) was C-terminally fused to SmBiT with a 15 amino acid flexible linker (GGSGGGGSGGSSSGGG), and the resulting construct referred to as Nb37-SmBiT. The C-terminal KRAS CAAX motif (SSSGGGKKKKKKSKTKCVIM) was N-terminally fused with LgBiT (LgBiT-CAAX). The Endofin FYVE domain (amino acid region Gln739-Lys806) was C-terminally fused with LgBiT (Endofin-LgBiT). $G\alpha_s$ (human, short isoform), Gβ1 (human), Gγ2 (human), and RIC8B (human, isoform 2) plasmids were inserted into pcDNA3.1 or pCAGGS expression plasmid vectors. INS-1 832/3 GLP-1R KO or GIPR KO cells were seeded in 6-well plates and co-transfected with 0.1 μg SNAP-GLP-1R or SNAP-GIPR, 0.5 μg $G\alpha_s$, Gβ1, and Gγ2, 0.1 μg RIC8B, 0.1 μg CAAX-LgBiT or 0.5 μg Endofin-LgBiT with 0.1 μg or 0.5 μg Nb37-SmBiT, respectively, with 0.8 μg pcDNA3.1 added to the former to equalize DNA content.

All NanoBiT and NanoBRET readings were obtained in a Flexstation 3 plate reader. Briefly, 24 hours after transfection, cells were detached, resuspended in NanoGlo Live Cell Reagent (Promega) with furimazine (1:20 dilution) and seeded into white 96-well half-area plates. For NanoBiTs, baseline luminescence was recorded for 5 minutes at 37 °C followed by 30 minutes with or without addition of GLP-1 or GIP at 100 nM for G protein and β-arrestin 2 recruitment assays, and at serial doses of up to 1 μM for the Nb37 bystander assays; readings were taken every 30 seconds or every minute, respectively. For NanoBRETs, baseline luminescent signals were recorded every minute at 460 nm (NanoLuc emission peak) and 535 nm (Venus emission peak) over 5 minutes at 37 °C, followed by 30 minutes with or without the addition of 100 nM GLP-1 or GIP. Readings were normalized to well baseline and then to average vehicle-induced signal to establish the agonist-induced effect. AUCs from response curves were calculated for each agonist concentration and fitted to four-parameter curves using Prism 9 (GraphPad).

Transfections

Transient transfection of plasmids was performed using Lipofectamine 2000 (Thermo Fisher) according to the manufacturer's instructions. Experiments were performed 24 hours after transfection unless otherwise indicated.

Receptor Degradation Assays

High-content microscopy assay

The assay was adapted from a previous description (23). The INS-1 832/3 SNAP-GLP-1R or SNAP-GIPR cells were seeded in complete medium in poly-D-lysine-coated black, clear-bottom plates. Once attached, cells were washed twice in PBS and incubated in fresh serum-free medium containing cycloheximide (50 μg/mL) to arrest protein translation. After 2 hours, agonists were added in reverse time order (the longest time point being 8 hours), with the medium replaced for the final 30 minutes of the experiment with complete medium containing 1 μM BG-OG to label total residual SNAP-GLP-1R or SNAP-GIPR. Wells were then washed 3X in HBSS and the microplate imaged by widefield microscopy, with quantification of total cellular receptor at each time point from segmented cell-containing regions as for the high-content internalization and recycling assays described above.

Degradation assays by immunoblotting

INS-1 832/3 SNAP-GLP-1R and SNAP-GIPR cells were seeded in 6-well plates (1.5 million per well) and cultured overnight prior to incubation in serum-free medium containing cycloheximide (50 μg/mL) for 2 hours. Cells were then incubated with or without 100 nM GLP-1 or GIP for 6 hours before being lysed in 1X TNE lysis buffer (20 mM Tris, 150 mM NaCl, 1 mM EDTA, 1% NP40, protease and phosphatase inhibitor cocktails) for 10 minutes at 4 °C followed by cell scraping and sonication (3X, 10 seconds each). The lysates were then frozen at −80 °C for 2 minutes, thawed, and centrifuged at 15 000 g for 10 minutes at 4 °C. The supernatants were collected, fractionated by SDS-PAGE in urea loading buffer (200 mM Tris HCl pH 6.8, 5% w/v SDS, 8 M urea, 100 mM DTT, 0.02% w/v bromophenol blue) and analyzed by Western blotting. SNAP-GLP-1R and SNAP-GIPR were detected with an anti-SNAP-tag rabbit polyclonal antibody (P9310S, New England Biolabs, RRID: AB_10631145, 1/1000) followed by goat anti-rabbit HRP secondary (ab6721, Abcam, RRID: AB_955447, 1/2000). Post-stripping,

tubulin was labeled with anti-α-tubulin mouse monoclonal antibody (T5168, Sigma, RRID: AB_477579, 1/5000) followed by sheep anti-mouse HRP secondary antibody (ab6808, Abcam, RRID: AB_955441, 1/5000). Blots were developed with the Clarity Western enhanced chemiluminescence (ECL) substrate system (BioRad) in a Xograph Compact X5 processor and specific band densities quantified in Fiji.

Measurement of Receptor Clustering by Time-Resolved Fluorescence Resonance Energy Transfer

The time-resolved fluorescence resonance energy transfer (TR-FRET) assay was performed as previously described (24). INS-1 832/3 SNAP-GLP-1R or SNAP-GIPR cells were labeled in suspension with 40 nM SNAP-Lumi4-Tb and 1 mM SNAP-Surface 649 (New England Biolabs, Hitchin, UK) for 1 hour at room temperature in complete medium. After washing, cells were resuspended in HBSS, and TR-FRET was monitored before and after addition of 100 nM GLP-1, GIP, or a mixture of GLP-1 and GIP at 37 °C in a Spectramax i3x plate reader in homogeneous time-resolved fluorescence (HTRF) mode. TR-FRET was quantified as the ratio of fluorescent signal at 665 nm to that at 616 nm, after subtraction of background signal at each wavelength.

Raster Image Correlation Spectroscopy

INS-1 832/3 SNAP-GLP-1R or SNAP-GIPR cells were seeded onto glass bottom MatTek dishes and surface-labeled with SNAP-Surface 488 (1 mM, 30 minutes at 37 °C). After washing, cells were imaged at the basal plasma membrane in HBSS with 10 mM HEPES at 37 °C either before or 5 minutes after stimulation with 100 nM GLP-1 or GIP, respectively. Time-lapse images of cells were acquired in a Zeiss LSM-780 inverted confocal microscope fitted with a 63x/1.2 NA water immersion objective. SNAP-Surface 488 was excited by a continuous wavelength laser at 488 nm and emission signal collected at 500 to 580 nm. The pinhole was set to one Airy unit. Optimized acquisition was performed to retrieve protein membrane diffusion values as described previously (25, 26). Images of 256 × 256 pixels at 8-bit depth were collected using 80 nm pixel size and 5 μsec dwell time, for 250 consecutive frames. To characterize the waist of the point spread function (PSF), 200 frames of freely diffusing recombinant EGFP (20 mM) were continuously collected, as described elsewhere (27, 28). Analysis was performed on images where intensity traces were not decreased continuously by 20% or more over 50 frames to avoid possible bleaching artifacts that would interfere in diffusion coefficient measurements. A moving average (background subtraction) of 10 was applied, so that artifacts due to cellular motion or very slow-moving particles were avoided. The obtained 2-dimensional (2D) autocorrelation map was then fitted, and a surface map obtained with the characterized PSF and the appropriate acquisition values for line time and pixel time. Three different regions of interest (ROI) were analyzed within the same cell, with the corresponding regions drawn employing a 64 × 64-pixel square. Raster image correlation spectroscopy (RICS) analysis was performed using the "SimFCS 4" software (Global Software, G-SOFT Inc., Champaign, IL) as described (29). RICS analysis was performed in ROIs of 64 × 64 pixels at 4 random cytoplasmic areas per cell using a moving average (background subtraction) of 10 to discard possible artifacts due to cellular motion and slow-moving particles passing through. The autocorrelation 2D map was then fitted to obtain a surface map that was represented as a 3D projection with the residuals on top. As a rule, we focused on those regions with intensity fluctuation events in which the intensity changes were following short increasing or decreasing steps, avoiding abrupt intensity decays or increases.

Cyclic AMP Homogeneous Time-Resolved Fluorescence Assays

INS-1 832/3 cells were stimulated with increasing concentrations of GLP-1 or GIP followed by lysis and cyclic AMP (cAMP) homogeneous time-resolved fluorescence (HTRF) immunoassay (cAMP Dynamic 2, 62AM4PEB, Cisbio, Codolet, France) according to the manufacturer's instructions. Results were expressed as basal fold increase responses and fitted to 3-parameter curves using Prism 9 (GraphPad).

Isolation and Culture of Pancreatic Islets

Nondiabetic mice of both sexes were used for islet isolation. Briefly, pancreata were infused via the common bile duct with RPMI-1640 medium containing 1 mg/mL collagenase from *Clostridium histolyticum* (Nordmark Biochemicals), dissected, and incubated in a water bath at 37 °C for 10 minutes. Islets were subsequently washed and purified using a Histopaque gradient (Histopaque-1119, 11191, Sigma-Aldrich, and Histopaque-1083, 10831, Sigma-Aldrich). Isolated islets were allowed to recover overnight at 37 °C in 5% CO_2 in RPMI-1640 supplemented with 10% FBS and 1% penicillin/streptomycin. All procedures were carried out in accordance with the regulations of the UK Home Office Animals (Scientific Procedures) Act and the Imperial College London guidelines for animal care. Animal protocols were approved by the Home Office Animals in Science Regulation Unit (ASRU) under Project License number PP7151519 to Dr. A. Martinez-Sanchez.

cAMP FRET Assays

CAMPER reporter mice (30), with conditional expression of the cAMP fluorescence resonance energy transfer (FRET) biosensor $^{T}EPAC^{VV}$ (31), were purchased from Jackson Laboratory (Stock No: 032205) and crossed with Pdx1-Cre^{ERT} mice (in house) to generate mice with inducible $^{T}EPAC^{VV}$ expression from pancreatic beta cells, used to isolate islets for ex vivo cAMP FRET assays. Isolated islets were treated overnight with 4-hydroxytamoxifen to induce biosensor expression prior to Matrigel encasing on MatTek glass bottom dishes and imaging by FRET between CFP (donor) and YFP (acceptor) with CFP excitation and both CFP and YFP emission settings in a Zeiss LSM-780 inverted confocal laser-scanning microscope and a 20X objective to capture time-lapse recordings with image acquisition every 6 seconds, and treatments manually added by pipetting. Specifically, islets were imaged in Krebs-Ringer bicarbonate-HEPES (KRBH) buffer (140 mM NaCl, 3.6 mM KCl, 1.5 mM $CaCl_2$, 0.5 mM $MgSO_4$, 0.5 mM NaH_2PO_4, 2 mM $NaHCO_3$, 10 mM HEPES, saturated with 95% O_2/5% CO_2; pH 7.4) containing 0.1% w/v bovine serum albumin (BSA) and 6 mM glucose (KRBH G6) for 1 minute, then agonist at 100 nM was added and imaged for 10 minutes before addition of 10 μM forskolin + 100 μM isobutyl methylxanthine (IBMX) for the final 2 minutes of the acquisition to record maximal

responses. Raw intensity traces for YFP and CFP fluorescence were extracted from whole islet ROIs using Fiji and YFP/CFP ratios calculated for each ROI and time point. Responses were plotted relative to the average fluorescence intensity per islet during the 6 mM glucose baseline period, before agonist addition.

Calcium Assays

Imaging of INS-1 832/3 cells or whole-islet Ca^{2+} dynamics was performed as follows: cells or Matrigel-encased islets from individual animals were loaded with the Ca^{2+} responsive dye Cal-520 AM (AAT Bioquest), pre-incubated for 1 hour in KRBH G6, and imaged in MatTek glass bottom dishes every 6 second at 488 nm using a Nikon Eclipse Ti microscope with an ORCA-Flash 4.0 camera (Hamamatsu) and Metamorph software (Molecular Devices) while maintained at 37 °C on a heated stage. Raw fluorescence intensity traces from cell-occupied areas or islet ROIs were extracted using Fiji. Responses were plotted relative to the average fluorescence intensity during the 6 mM glucose baseline period, before agonist addition.

Insulin Secretion Assays

INS-1 832/3 cells were seeded in a 48-well plate and incubated in 3 mM glucose in full medium overnight before incubation with 11 mM glucose ± GLP-1/GIP at 100 nM in KRBH buffer containing 0.1% w/v BSA at 37 °C. At the end of the treatments, the supernatant containing the secreted insulin was collected, centrifuged at 1000*g* for 3 minutes, and transferred to a fresh tube. To determine total insulin content, cells were lysed using KRBH buffer + 1% w/v BSA + 1% v/v Triton X-100 (Sigma). The lysates were sonicated 3 × 10 seconds in a water bath sonicator and centrifuged at 10 000*g* for 10 minutes, and the supernatants collected. The samples were stored at −20 °C until the insulin concentration was determined using an Insulin Ultra-Sensitive HTRF Assay kit (62IN2PEG, Cisbio, Codolet, France) according to the manufacturer's instructions.

Statistical Analyses

All data analyses and graph generation were performed with GraphPad Prism 9.0. The statistical tests used are indicated in the corresponding figure legends. The number of replicates for comparisons represents biological replicates. Technical replicates within biological replicates were averaged prior to statistical tests. Data are represented as mean ± SEM. The *P* value threshold for statistical significance was set at .05.

Results

We first analyzed the trafficking characteristics of both receptors following stimulation with their cognate full-length endogenous agonists, GLP-1(7-36)NH_2 and GIP(1-42), using rat INS-1 832/3 beta cells in which the endogenous incretin receptor was deleted and the equivalent SNAP-tagged human receptor exogenously expressed (INS-1 832/3 SNAP-GLP-1R or SNAP-GIPR cells). Note that surface expression levels of SNAP-GLP-1R and SNAP-GIPR were similar within these 2 cell models (Supplemental Fig. 1A) (32). DERET assays, which detect disappearance of the receptor by a loss of TR-FRET signal between the receptor extracellular domain (ECD) and the extracellular buffer (24), revealed stark differences in the degree of internalization between the 2 receptors following stimulation with their native agonists, with the GLP-1R achieving approximately 3 times more internalization in the first hour poststimulation with 100 nM GLP-1 compared with the GIPR for the same stimulation period with 100 nM GIP (Supplemental Fig. 1B and 1C) (32). Notably, there was negligible GLP-1R internalization in response to GIP, and vice versa, and no significant change to internalization for either receptor when using both agonists combined. Greater internalization of GLP-1R than of GIPR was observed across a wide concentration range (Fig. 1A and Supplemental Fig. 1D) (32). Analysis of the rate of change of DERET signal indicated that GLP-1R endocytosis was significantly faster (Fig. 1B). We corroborated these findings by high-content microscopy analysis of receptor internalization in the same cells (Fig. 1C), with significantly less internalization of GIPR compared with GLP-1R when stimulated with their respective endogenous agonists.

In concordance with these results, 30 minutes of stimulation with the fluorescently labeled agonist GLP-1-FITC (33) resulted in the near complete co-internalization of SNAP-GLP-1R and fluorescent ligand, while the equivalent treatment with GIP-FITC led to only partial SNAP-GIPR endocytosis, with the receptor still clearly visible at the plasma membrane (Fig. 1D and Supplemental Fig. 1E) (32). Moreover, when both receptors harboring different N-terminal tags (so that they could be differentially labeled) were expressed together in wild-type (WT) INS-1 832/3 cells, HALO-GLP-1R did again show faster internalization vs SNAP-GIPR following stimulation with a mixture of GLP-1 and GIP (Supplemental Fig. 2) (32). Finally, using alternative fluorescent conjugates labeled with TMR, the amount of TMR-labeled agonist intracellular accumulation during the first 5 minutes of stimulation for each receptor correlated with the previously shown receptor internalization results in INS-1 832/3 SNAP-GLP-1R/SNAP-GIPR cell lines (Supplemental Fig. 3A and 3B) (32). Consistently, in WT mouse primary islets, GIP-TMR could be detected at the plasma membrane, while GLP-1-TMR was predominantly localized in punctate structures reminiscent of endosomes after 15 minutes of agonist stimulation (Fig. 1E). As a control, GIP-TMR signal at the plasma membrane was absent in islets from *Gipr*$^{-/-}$ (KO) mice (34) labeled in parallel with the same concentration of GIP-TMR, demonstrating specificity of labeling in WT islets. Of note, signal was significantly lower for GIP- vs GLP-1-TMR (quantified in Fig. 1F), with GIP-TMR signal virtually undetectable in islets at a concentration of 100 nM (not shown). This result suggests reduced levels of endogenous GIPR vs GLP-1R in mouse islets and correlates with previously published RNAseq data indicating higher levels of beta cell *Glp1r* vs *Gipr* mRNA expression in those islets (35). Additional experiments were performed using dispersed mouse islet cells, which also showed markedly reduced that GIP-TMR uptake compared with GLP-1-TMR (Supplemental Fig. 3C) (32).

We also analyzed the level of receptor recycling back to the plasma membrane after internalization in INS-1 832/3 SNAP-GLP-1R or SNAP-GIPR cells by high-content microscopy after stimulation with 100 nM GLP-1 or GIP, respectively, and detected significantly increased recycling rates for the GIPR compared with the GLP-1R (Fig. 1G), an observation that correlated with sustained SNAP-GIPR, but not SNAP-GLP-1R, colocalization with the recycling factor SNX27 (36) fused to EGFP (Fig. 1H). To determine the

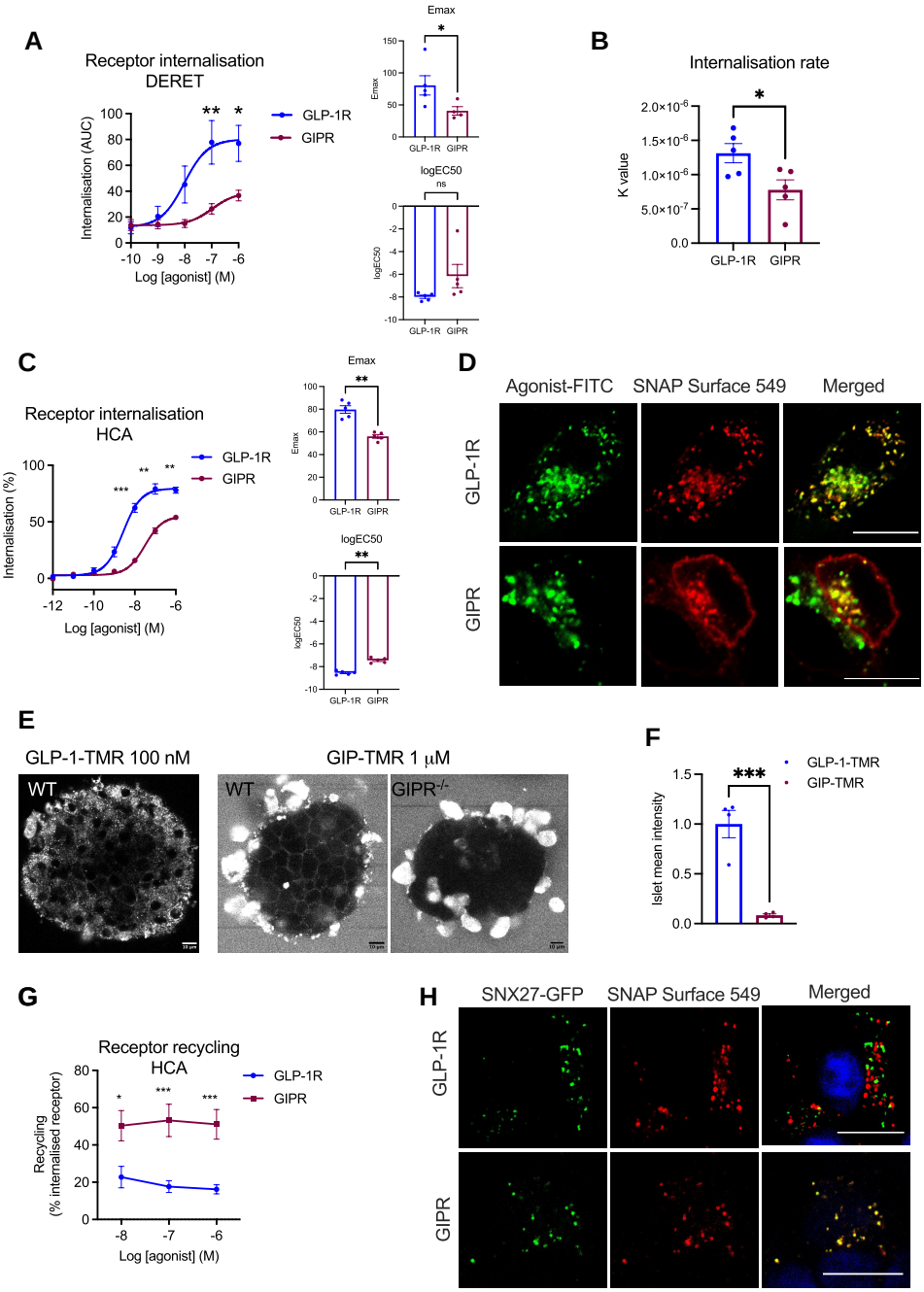

Figure 1. Beta cell GLP-1R vs GIPR trafficking patterns. (A) Internalization AUC dose response curves from DERET assays in INS-1 832/3 SNAP-GLP-1R vs SNAP-GIPR cells stimulated with the indicated concentrations of GLP-1 or GIP, respectively. Results were fitted to a 3-parameter dose response curve to obtain Emax and logEC50 for both receptors, with comparisons between these parameters included; $n = 5$. (B) Rates of GLP-1R vs GIPR internalization (k values) derived from (A) by one-phase association (with Y0 = 0) of baseline-deleted DERET data; $n = 5$. (C) GLP-1R vs GIPR internalization dose response curves measured by high-content microscopy assay (HCA) in the same cells as above. Results fitted and Emax and logEC50 comparisons included as above; $n = 5$. (D) Confocal microscopy analysis of SNAP-GLP-1R vs SNAP-GIPR (red, middle panels) localization following 30 minutes stimulation with 100 nM GLP-1-FITC or GIP-FITC (green, left panels), respectively, in the same cells as above. (E) Confocal microscopy analysis of isolated intact mouse islets stimulated with fluorescently labeled agonists as indicated: WT islets were imaged following stimulation with 100 nM GLP-1-TMR, while both WT and GIPR$^{-/-}$ (KO) islets were imaged following stimulation with 1 μM GIP-TMR. (F) Quantification of surface GLP-1R vs GIPR levels in WT mouse islets using fluorescent agonist uptake data from (E); data corrected for binding affinity differences between both agonists; $n = 4$. (G) GLP-1R vs GIPR recycling dose response curves measured by high-content microscopy assay (HCA) in cells from (C); $n = 5$. (H) Confocal microscopy analysis of SNAP-GLP-1R vs SNAP-GIPR (red, middle panels) colocalization with SNX27-GFP (green, left panels) following 3 hours stimulation with 100 nM GLP-1 or GIP, respectively, in the same cells as above. Nuclei (DAPI), blue. Data are mean ± SEM, compared by paired or unpaired *t* tests, or two-way ANOVA with Sidak's post hoc test; $^*P < .05$, $^{**}P < .01$, $^{***}P < .001$; size bars: 10 μm.

intracellular destination of internalized GLP-1Rs/GIPRs more precisely, we performed concentration response bystander NanoBRET assays using C-terminal NanoLuc-fused SNAP-tagged GLP-1R vs GIPR and either KRAS-Venus (plasma membrane) or Rab5-Venus (early endosome) co-expressed transiently in INS-1 832/3 cells (Fig. 2). In these experiments, we again observed increased propensity for plasma membrane retention of the GIPR compared with the

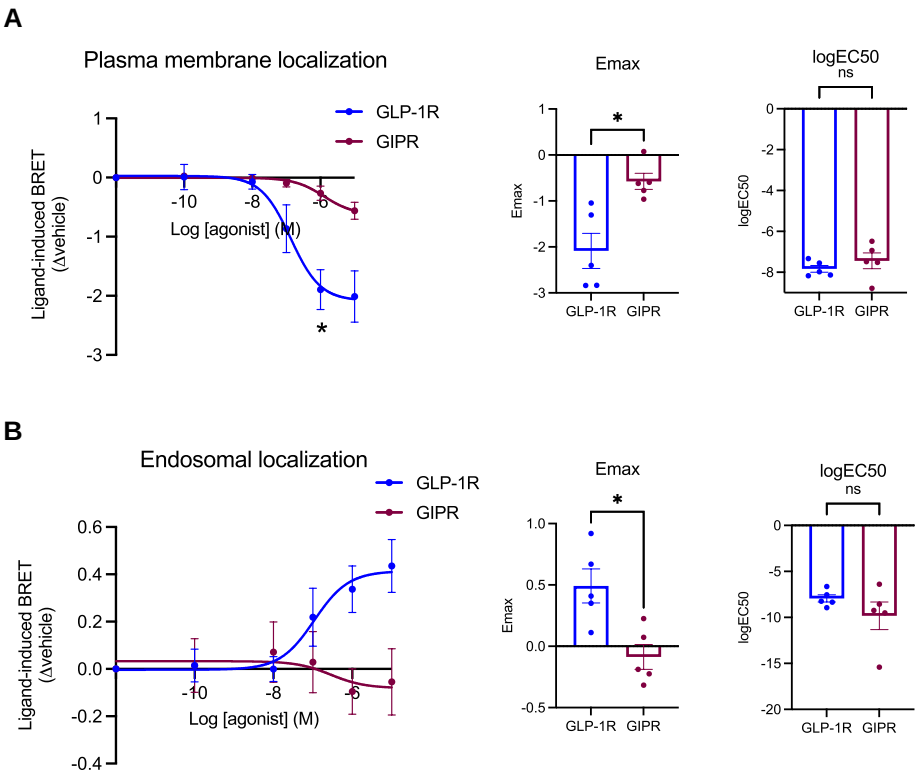

Figure 2. Endosomal vs plasma membrane localization of GLP-1R compared with GIPR in beta cells. (A) GLP-1R vs GIPR plasma membrane localization dose response curves from NanoBRET assays performed in INS-1 832/3 GLP-1R KO vs GIPR KO cells transiently expressing KRAS-Venus and GLP-1R- or GIPR-NanoLuc, after stimulation with the indicated concentrations of GLP-1 or GIP, respectively; results were fitted to 3-parameter dose response curves to obtain Emax and logEC50 for both receptors, with comparisons between these parameters included; $n = 5$. (B) As for (A) but for GLP-1R vs GIPR endosomal localization dose response curves from NanoBRET assays performed in INS-1 832/3 GLP-1R KO vs GIPR KO cells transiently expressing Rab5-Venus and GLP-1R- or GIPR-NanoLuc, after stimulation with the indicated concentrations of GLP-1 or GIP, respectively; $n = 5$. Data are mean ± SEM, compared by paired *t* tests or two-way ANOVA with Sidak's test; $^*P < .05$.

GLP-1R, with reduced maximal internalization responses but no changes in potency (Fig. 2A). Agonist-mediated redistribution of GLP-1R to Rab5-positive early endosomes was clearly detectable, but virtually absent for the GIPR in this system (Fig. 2B). In broad agreement with these results, using stable INS-1-SNAP-GLP-1R or -GIPR cells, the majority of SNAP-GLP-1R signal could be detected in Rab5-Venus-positive endosomes after 10 minutes of stimulation with 100 nM GLP-1, while a sizable amount of SNAP-GIPR was still present at the plasma membrane following stimulation with 100 nM GIP; with the fraction of internalized GIPRs nevertheless also localized to Rab5-Venus-positive endosomes (Supplemental Fig. 4) (32).

We have previously found that agonist-induced GLP-1R internalization is preceded by receptor clustering at the plasma membrane (24). We therefore investigated whether the degree of clustering for each incretin receptor in a beta cell setting would reflect the differences observed in their internalization profiles (Fig. 3). Employing RICS (27), we observed receptor clustering tendencies in INS-1 832/3 SNAP-GLP-1R or SNAP-GIPR cells labeled with the SNAP-Surface 488 probe under vehicle conditions as well as after 5 minutes of stimulation with 100 nM GLP-1 or GIP, respectively (Fig. 3A). Quantification of receptor diffusion coefficients revealed that, while the GIPR exhibits slower basal diffusion, suggesting more clustering than the GLP-1R under vehicle conditions [a phenotype that correlates with our previously observed increased propensity for this receptor to segregate to cholesterol-rich lipid nanodomains under basal conditions (24)], agonist stimulation resulted in marked slowing of diffusion for both receptors (Fig. 3B). Additionally, TR-FRET experiments suggested increased GLP-1R clustering when stimulated with GLP-1 (Fig. 3C), an effect that could not be detected following GIP stimulation of the GIPR (Fig. 3D). Moreover, clustering was not detectable when inverting the cognate agonists and no significant increases were detected by co-application of both agonists for each of the INS-1 832/3 receptor cell models (Fig. 3C and 3D).

We next analyzed the level of receptor degradation and lysosomal localization with a series of assays for both incretin receptors in INS-1 832/3 cells. We first assessed the total level of SNAP-GLP-1R vs SNAP-GIPR in INS-1 832/3 SNAP-GLP-1R or SNAP-GIPR cells in vehicle conditions or following 3-hour stimulation with 100 nM GLP-1 or GIP by Western blotting (Fig. 4A and 4B). This experiment showed an increased propensity for degradation of the GLP-1R when compared with the GIPR. We next quantified the level of receptor degradation using a high-content microscopy approach in which remaining total cellular SNAP-tag receptor is labeled after agonist incubation using the cell-permeable SNAP-tag probe BG-OG (23), and again observed faster receptor degradation for the GLP-1R vs the GIPR (Fig. 4C). Finally, we also quantified the colocalization between each SNAP-tagged receptor and the lysosomes, finding significantly higher lysosomal targeting for the GLP-1R compared with the GIPR (Fig. 4D and Supplemental Fig. 5) (32), a pattern that correlates with a reduced tendency for the GLP-1R vs the GIPR to localize to Rab11-positive recycling compartments following cognate agonist exposure (Supplemental Fig. 6) (32).

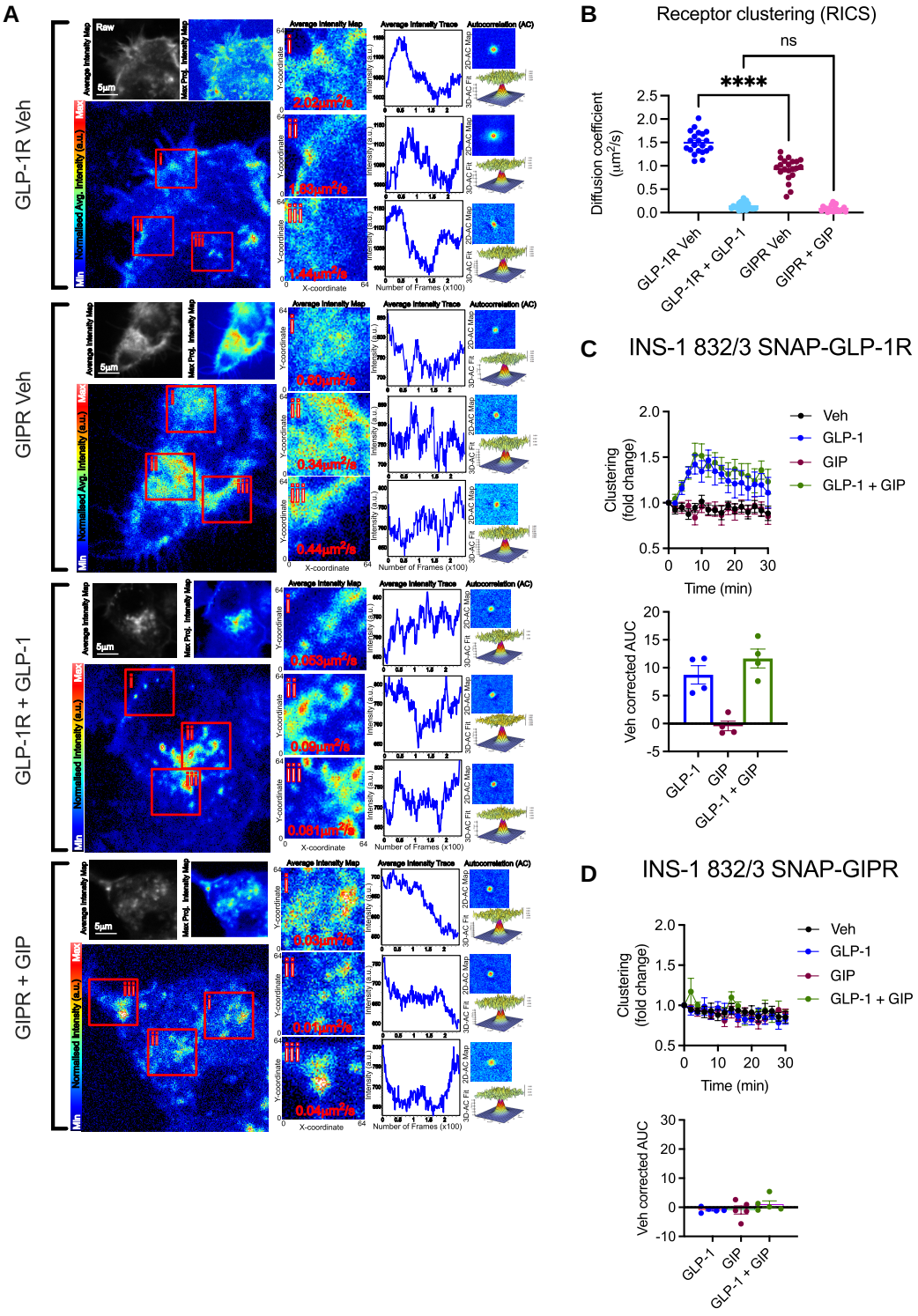

Figure 3. GLP-1R vs GIPR clustering propensities in beta cells. (A) Representative images from RICS analysis of GLP-1R vs GIPR clustering, showing SNAP-Surface 488-labeled GLP-1Rs or GIPRs imaged in the basolateral plane of INS-1 832/3 SNAP-GLP-1R vs SNAP-GIPR cells after 5 minutes treatment in vehicle (Veh) and either 100 nM GLP-1 or GIP. Diffusion coefficients for individual ROIs are indicated on each image, with corresponding intensity traces, as well as 2D and fitted 3D autocorrelation maps for each ROI, are also depicted. (B) Average RICS diffusion coefficients for each receptor and treatment for each cell analyzed from $n = 4$ experiments. (C) GLP-1R clustering kinetics measured by TR-FRET in INS-1 832/3 SNAP-GLP-1R cells treated with 100 nM agonist as indicated, with vehicle-corrected AUCs included; $n = 4$. (D) GIPR clustering kinetics measured by TR-FRET in INS-1 832/3 SNAP-GIPR cells treated with 100 nM agonist as indicated, with vehicle-corrected AUCs included; $n = 4$. Data are mean ± SEM, compared by one-way ANOVA with Sidak's test; $^{****}P < .0001$; ns: non-significant.

Having elucidated the main trafficking characteristics of both receptors, we next determined the coupling of each incretin receptor with specific signaling mediators, including $G\alpha_s$, $G\alpha_q$, $G\alpha_i$, and β-arrestin 2 in INS-1 832/3 cells using NanoBiT complementation assays (Fig. 5). As previously shown by our group using analogous assays in HEK293T cells

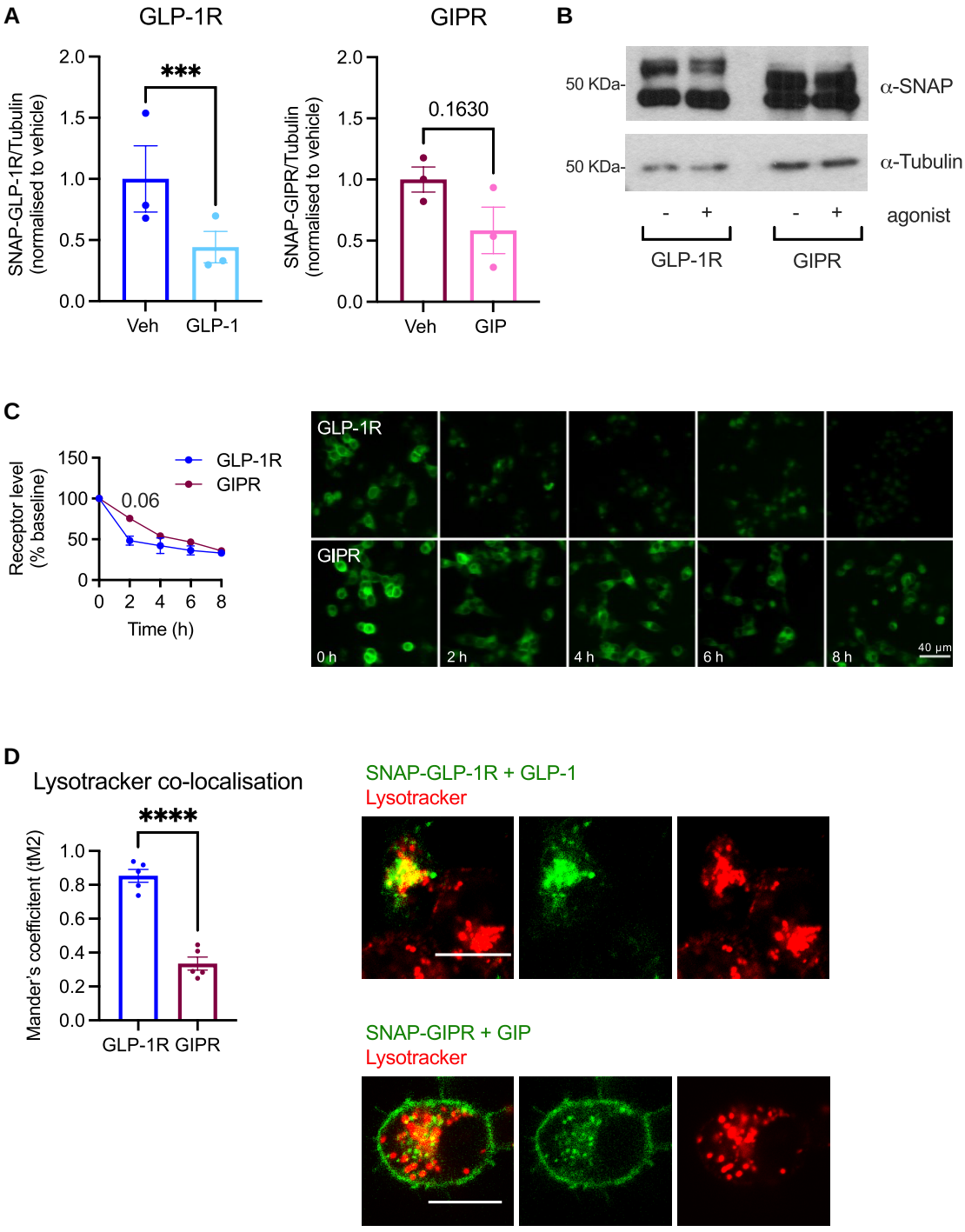

Figure 4. Beta cell GLP-1r vs GIPR degradation propensities. (A) Western blot assessment of SNAP-GLP-1R or GIPR over tubulin levels in INS-1 832/3 SNAP-GLP-1R or SNAP-GIPR cells with or without stimulation with 100 nM GLP-1 or GIP, respectively, for 6 hours in the presence of the protein synthesis inhibitor cycloheximide; $n = 3$. (B) Representative Western blot results from (A). Note that the top bands were used to quantify the SNAP-receptor levels, as they correspond to the glycosylated forms of the receptors, known to be biologically active and correctly inserted at the plasma membrane (24). (C) Percentage of GLP-1R vs GIPR, labeled with the cell-permeable SNAP-tag probe BG-OG, and corresponding representative images from INS-1 832/3 SNAP-GLP-1R or SNAP-GIPR cells with or without stimulation with 100 nM GLP-1 or GIP, respectively, for the indicated times in the presence of cycloheximide; $n = 4$. (D) Percentage of co-localization (Mander's coefficient) and representative images of SNAP-GLP-1R vs -GIPR (labeled with SNAP-Surface 649) with Lysotracker Green in INS-1 832/3 SNAP-GLP-1R or SNAP-GIPR cells stimulated with 100 nM GLP-1 or GIP for 1 hour; $n = 5$. Data are mean ± SEM, compared by ratio-paired or unpaired *t* test or two-way ANOVA with Sidak's post hoc test; $^{***}P < .001$, $^{****}P < .0001$.

(37), the GLP-1R was preferentially coupled to $G\alpha_s$, followed by $G\alpha_q$ and with minimum coupling to $G\alpha_i$ proteins in response to GLP-1 stimulation (Fig. 5A), while GIPR responses to GIP were markedly reduced for all readouts compared with GLP-1R (Fig. 5B). As the values for $G\alpha_s$ recruitment to the GIPR were almost as low as those obtained for $G\alpha_i$ using this NanoBiT approach, we decided to verify whether the $G\alpha_s$ results would be consistent when using a potentially

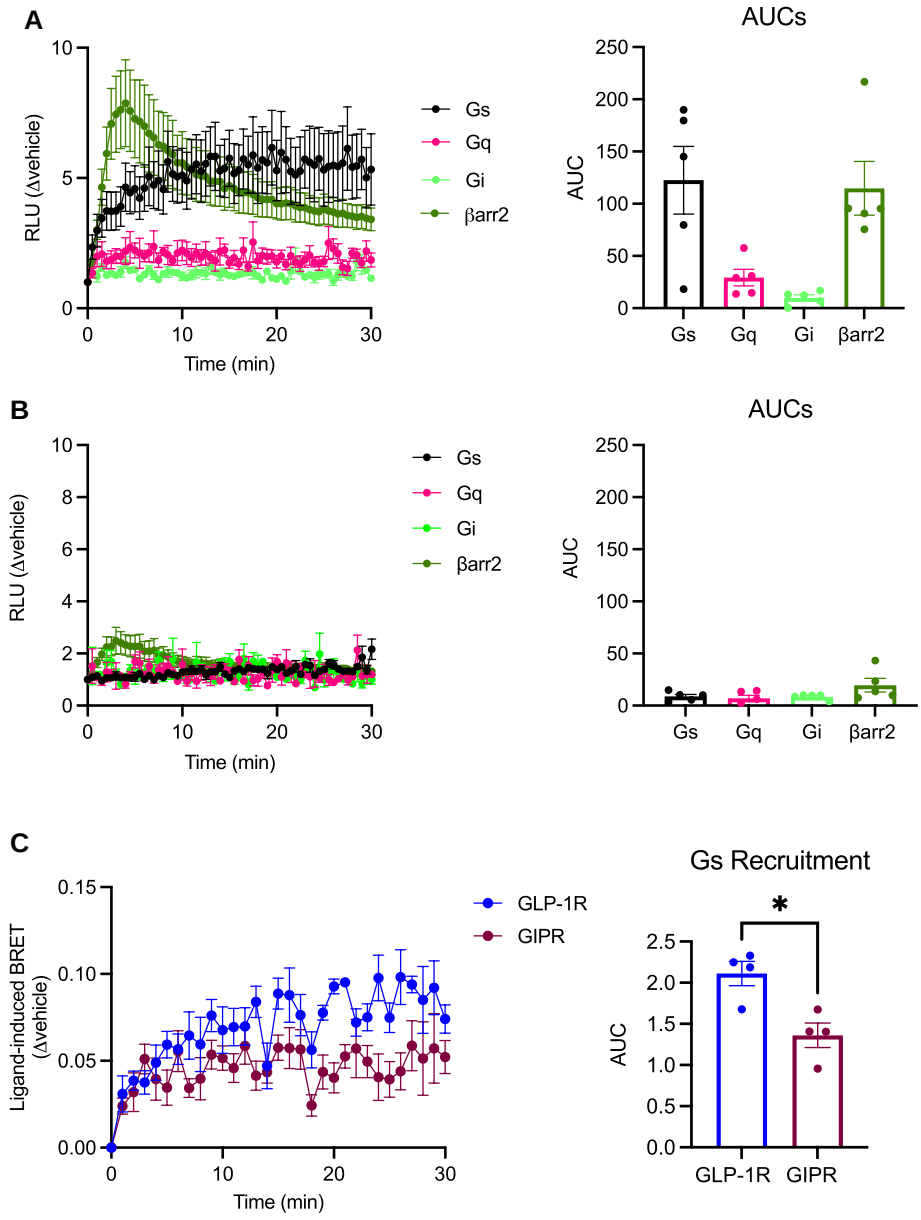

Figure 5. Beta cell GLP-1R vs GIPR G protein subtype and β-arrestin 2 recruitment characteristics. (A) Kinetics of $G\alpha_s$, $G\alpha_q$, $G\alpha_i$, and β-arrestin 2 recruitment to the GLP-1R assessed by NanoBiT complementation assay in INS-1 832/3 GLP-1R KO cells transiently expressing GLP-1R-SmBiT and the corresponding mini-G protein subtype or β-arrestin 2. Responses to 100 nM GLP-1 normalized to vehicle and corresponding AUCs are shown; $n = 5$. (B) Kinetics of $G\alpha_s$, $G\alpha_q$, $G\alpha_i$, and β-arrestin 2 recruitment to the GIPR assessed by NanoBiT complementation assay in INS-1 832/3 GIPR KO cells transiently expressing GIPR-SmBiT and the corresponding mini-G protein subtype or β-arrestin 2. Responses to 100 nM GIP normalized to vehicle and corresponding AUCs are shown; $n = 5$. (C) NanoBRET assessment of GLP-1R vs GIPR recruitment of $G\alpha_s$, performed in INS-1 832/3 GLP-1R KO vs GIPR KO cells transiently expressing mini-Gs-Venus and either GLP-1R- or GIPR-NanoLuc, after stimulation with 100 nM GLP-1 or GIP, respectively, with corresponding AUCs also shown; $n = 4$. Data are mean ± SEM, compared by paired *t* test; $^{***}P < .05$.

more sensitive assay, namely a method based on NanoBRET between C-terminal NanoLuc-fused receptor and mini-Gs-Venus in the same cells as above (Fig. 5C). Results with this method again showed significantly reduced $G\alpha_s$ recruitment to the GIPR compared to the GLP-1R, although the difference between both receptors was less pronounced than previously found by NanoBiT complementation.

Next, to determine the spatiotemporal pattern of $G\alpha_s$ activation elicited by the 2 receptors, we employed a recently developed bystander NanoBiT signaling assay based on the recruitment of activated $G\alpha_s$-recognizing nanobody 37 (Nb37) to plasma membrane and endosomal locations in response to specific agonist stimulations (38) (Fig. 6 and Supplemental Fig. 7) (32). While the assay showed no significant differences in the recruitment of Nb37 to active GLP-1Rs or GIPRs within the plasma membrane (Fig. 6A and Supplemental Fig. 7A) (32), there was a clear difference in GLP-1R vs GIPR endosomal activity, including a profoundly reduced GIPR Emax response despite increased potency for endosomal signaling with this receptor compared with the GLP-1R (Fig. 6B and Supplemental Fig. 7B) (32).

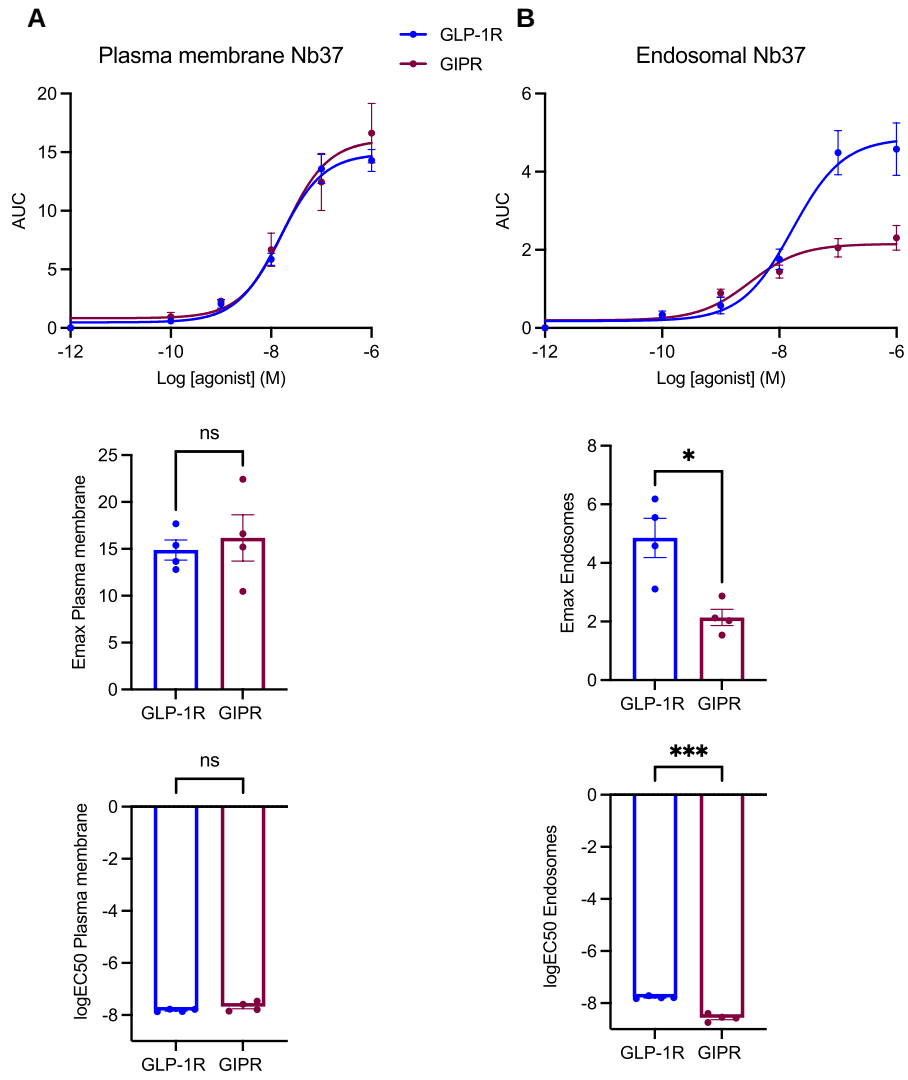

Figure 6. GLP-1R vs GIPR endosomal vs plasma membrane activity in beta cells. (A) GLP-1R vs GIPR plasma membrane activity dose response curves from bystander NanoBiT signaling assays performed in INS-1 832/3 GLP-1R KO vs GIPR KO cells transiently expressing Nb37-SmBiT, LgBiT-CAAX and SNAP-GLP-1R or -GIPR, after stimulation with the indicated concentrations of GLP-1 or GIP, respectively; 30-minute AUC for each agonist concentration tested were fitted to 3-parameter dose response curves to obtain plasma membrane Emax and logEC50 for both receptors, with comparisons between these parameters included; $n = 4$. (B) As for (A) but for GLP-1R vs GIPR endosomal activity in INS-1 832/3 GLP-1R KO vs GIPR KO cells transiently expressing Nb37-SmBiT, Endofin-LgBiT and SNAP-GLP-1R or -GIPR, after stimulation with the indicated concentrations of GLP-1 or GIP, respectively; $n = 4$. Data are mean ± SEM, compared by paired *t* tests; $^{*}P < .05$, $^{***}P < .001$.

Finally, we determined the downstream signaling effects of both incretin receptors when stimulated with their native cognate agonists in beta cells (Fig. 7), and found a near-significant increase in cAMP response to 100 nM GIP compared with GLP-1 stimulation in wild-type INS-1 832/3 cells (Fig. 7A), a tendency replicated in primary mouse islet beta cells (Fig. 7B). For intracellular calcium influx in INS-1 832/3 cells, while there was an initial trend for a decreased GIPR compared with GLP-1R response during the first minute of stimulation, this tendency was reversed for the following 4 minutes of agonist exposure, resulting in a zero net difference between both receptors (Fig. 7C). However, in primary islets, there was a significant increase in calcium influx in response to GIP vs GLP-1 stimulations (Fig. 7D). Finally, insulin secretion assays performed in INS-1 832/3 cells showed a nonsignificant tendency toward improvement following GIP compared with GLP-1 exposure, with responses being specific for either the GIPR (for GIP) or the GLP-1R (for GLP-1), as they were abolished in the absence of each receptor in the corresponding GLP-1R or GIPR KO cells (Fig. 7E).

Discussion

In this study, we have established the main pattern of spatiotemporal signaling for each incretin receptor in a relevant cellular system, primarily INS-1 832/3 rat beta cells (with selected assays in primary mouse islets), where the receptors are expressed endogenously (see Table 1 for a summary of the main results). We have found marked differences in the trafficking and signaling characteristics from the 2 receptors, with GIPR associated with significantly reduced internalization and degradation propensities but increased plasma membrane recycling when compared with GLP-1R by several different techniques, a pattern that correlates with reduced

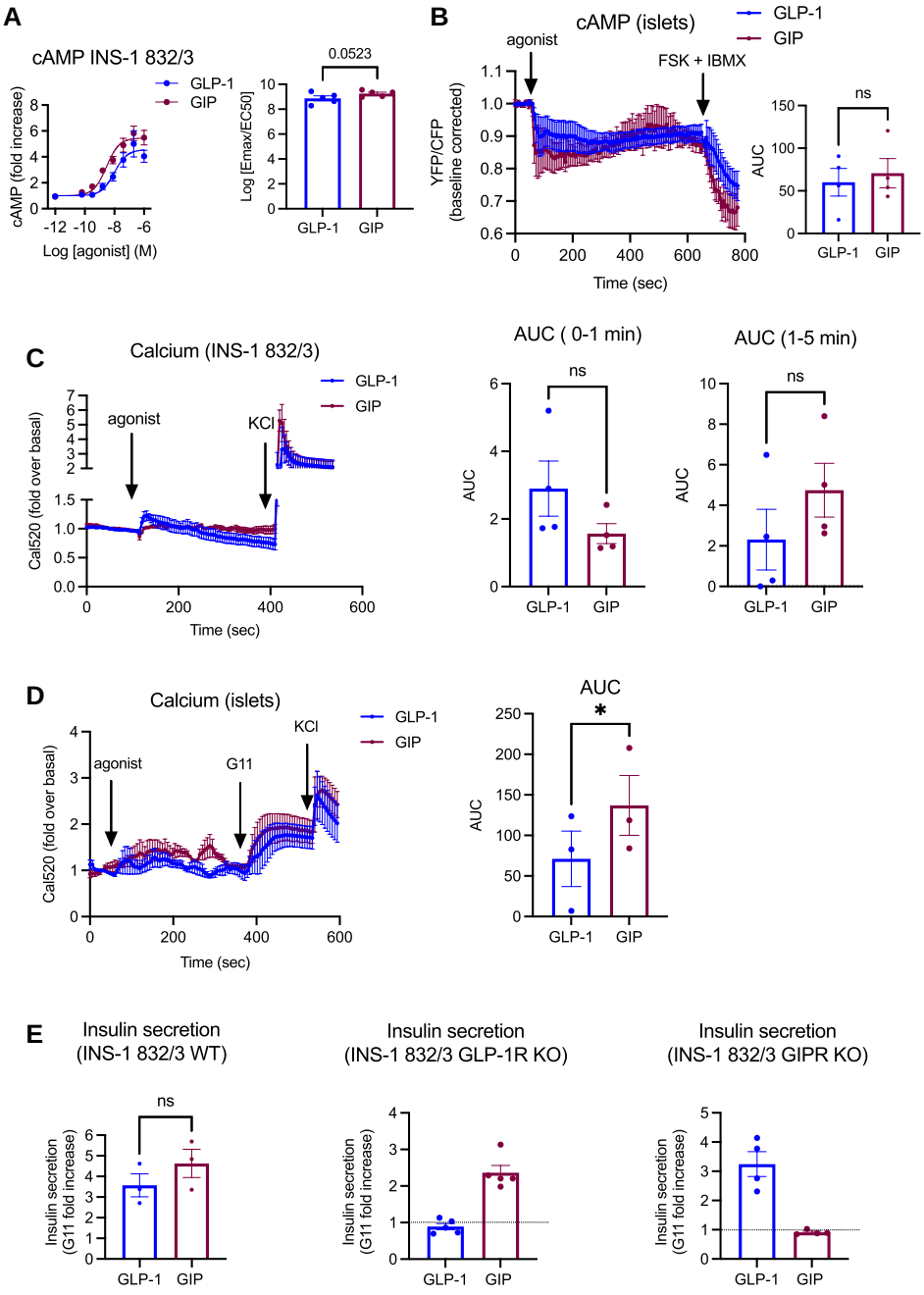

Figure 7. Functional analysis of GLP-1R vs GIPR signaling in beta cells. (A) cAMP dose response curves to GLP-1 vs GIP assessed in INS-1 832/3 cells by HTRF assay; results were fitted to 3-parameter dose response curves to obtain plasma membrane Emax and logEC50 for both receptors, depicted here combined as log(Emax/EC50) for each receptor; $n = 5$. (B) cAMP FRET responses to 100 nM GLP-1 or GIP from isolated and 4-hydroxytamoxifen-treated Pdx1-Cre^{ERT}/CAMPER mouse islets; including agonist AUCs calculated for each receptor; $n = 4$. (C) INS-1 832/3 calcium responses (using the calcium indicator Cal520-AM) to 100 nM GLP-1 or GIP, including agonist AUCs calculated for 0-1 minute and 1-5 minutes responses for each receptor; $n = 4$. (D) Calcium responses to 100 nM GLP-1 vs GIP from purified WT mouse islets loaded with Cal520-AM, including agonist AUCs for each receptor; $n = 4$. (E) Insulin secretion responses to 100 nM GLP-1 vs GIP, expressed as fold increases to 11 mM glucose (G11) secretion levels from INS-1 832/3 WT ($n = 3$), GLP-1R KO ($n = 5$) and GIPR KO ($n = 4$) cells. Data are mean ± SEM, compared by paired *t* tests; *$P < .05$; ns, nonsignificant.

activity from endosomes but no significant differences in plasma membrane activity. While the trafficking of the GIPR has been examined before in heterologous HEK293/HEK293T cells (37, 39), this is to our knowledge the first in-depth examination of these patterns in endogenous receptor-expressing pancreatic beta cells, including spatiotemporal assessment of signaling. Interestingly, while the net effect of these trafficking variations appears to be an increased level of sustained GIPR localization at the plasma membrane, we were nevertheless able to detect some intracellular GIP-FITC signal accumulation after 30 minutes of agonist stimulation (although intracellular GIP-TMR, unlike GLP-1-TMR, was negligible at

Table 1. Summary of trafficking, coupling, and cellular outputs of GLP-1R vs GIPR in response to cognate agonists

	GLP-1R	GIPR
Trafficking		
Islet surface expression	+	+
Internalization	+	+
Recycling	+	+
Endosome localization	+	−
Clustering (vehicle)	−	+
Clustering (stimulated)	+	+
Degradation	+	+
Coupling		
Gαs	+	+
Gαq	+	−
Gαi	−	−
β-arrestin 2	+	+
Plasma membrane Gαs	+	+
Endosome Gαs	+	+
Beta cell responses		
cAMP (INS-1 832/3)	+	+[a]
cAMP (islet beta cells)	+	+[a]
Calcium (INS-1 832/3)	+	+
Calcium (islets)	+	+
Insulin secretion (INS-1 832/3)	+	+[a]

[a]nonsignificant

the shorter time point of 5 minutes poststimulation), pointing toward active GIPRs continuously shuttling in and out of cells by a slow internalizing coupled to a rapidly recycling pathway, depositing their agonist in an intracellular location prior to returning to the plasma membrane, in a mechanism reminiscent to that previously observed by us for the related glucagon receptor (GCGR) (38).

A previous study from our group performed in HEK293T cells also reported reduced internalization propensity for the GIPR vs the GLP-1R in response to stimulation with their corresponding native agonists, a pattern that correlated with reduced recruitment of β-arrestin 2 to the GIPR (37), an effect already observed before in a prior study from a separate group performed in HEK293 cells (40). Here, we again observe reduced propensity for β-arrestin 2 recruitment by the GIPR in a beta cell context. The role of β-arrestins on incretin receptor trafficking and signaling has previously been investigated from several angles, for example by the use of biased agonists with different capabilities for β-arrestin recruitment (13, 37), using in vivo conditional β-arrestin 2 knockout mouse models, or with in vitro cell systems with deleted β-arrestin 1/2 expression (24, 37). In all these instances, β-arrestin recruitment closely correlated with the degree of incretin receptor internalization, but alterations in β-arrestin expression levels or complete β-arrestin deletion did not lead to significant effects in receptor endocytosis, but rather resulted in the prolongation of cAMP/PKA signaling duration, suggesting that the main effect of this important signaling mediator lies in the steric hindrance caused by its binding to the receptor, leading to reduced access of $G\alpha_S$ to its binding pocket and promoting homologous receptor desensitization (41). Of note, similar reduced GIPR vs GLP-1R β-arrestin recruitment and internalization into a Rab5-positive endosomal compartment were also apparent in a separate study (39), although in this instance the authors focused on the comparison between responses from single and dual agonists such as tirzepatide or MAR709 for each receptor rather than performing a direct comparison of both receptor responses. Also interestingly, we have previously observed that *in vivo* GIPR responses are less affected by β-arrestin 2 deletion specifically from pancreatic beta cells (unpublished), suggesting a reduced reliance on β-arrestin 2 to regulate GIPR signaling effects in the pancreas.

Despite the abovementioned effects, the GIPR seems not only to be associated with reduced β-arrestin 2 recruitment but paradoxically with a general dampening in the recruitment of other downstream effectors including $G\alpha_s$ and $G\alpha_q$ proteins when measured as fold increases to vehicle levels, matching previous observations in HEK293T cells (37). While the reasons behind this effect are not fully elucidated, it is important to point out that the GIPR has previously been found to have significantly higher levels of basal activity vs the GLP-1R (40). Accordingly, we found increased basal association of this receptor with cholesterol-rich plasma membrane nanodomains (24), which are signaling hotspots rich in G proteins (42). Consistently, we now find significantly reduced rates of basal diffusion for GIPR vs GLP-1R, indicative of increased basal clustering, which correlate with an overall reduction in clustering fold increases in response to GIPR stimulation, again suggesting higher basal activity for the GIPR compared with the GLP-1R. This observation could potentially contribute to the disconnect between the overall reduced level of $G\alpha_s$ and $G\alpha_q$ recruitment to the GIPR, measured as fold increases in stimulated over vehicle conditions, and the observed tendency toward increased cAMP, calcium, and insulin secretion responses to GIP vs GLP-1 in INS-1 832/3 cells. Also of note, these tendencies are present despite the measured loss of recruitment of active $G\alpha_s$ to endosomal compartments, suggesting that, as previously observed for the GLP-1R when stimulated with biased compounds affecting its capacity for endosomal localization and activity (13, 43), the plasma membrane is the main contributor to the overall signaling output of incretin receptors. This disconnect also highlights the existence of powerful mechanisms of signal amplification associated with the GIPR, potentially related to differential interactions with downstream signaling mediators vs the GLP-1R. It is worth noting, however, that direct comparisons between different recruitment and activity assays are problematic due to potential differences in receptor vs effector expression levels leading to variations in stoichiometry as well as different dynamic ranges for each specific assay which might complicate their interpretation. Another possible limitation of our study relates to the use of clonal INS-1 832/3 sublines with either GLP-1R or GIPR inactivation, although preservation of cellular responses to the remaining incretin receptor in GLP-1R and GIPR KO cells, as demonstrated in Fig. 7E, increases our confidence that these clones have retained the necessary machinery for incretin-dependent potentiation of insulin secretion. Nevertheless, it is interesting to note that the GIPR also appears to signal more prominently than the GLP-1R in primary islets, where we measured a nonsignificant tendency toward increased cAMP and a significant increase in calcium responses to GIP vs GLP-1 despite a 12-fold reduction in endogenous surface GIPR vs GLP-1R

levels estimated in WT mouse islets in this study by quantification of TMR-labeled agonist uptake. Here it is also important to highlight that while cAMP responses were measured in islets from mice expressing a cAMP biosensor specifically from beta cells, calcium responses were acquired from whole islets and therefore also included responses from other islet endocrine cell types, which might explain the differences in the response observed in INS-1 832/3 cells.

In summary, we have described here significant differences in the trafficking and spatiotemporal signaling propensities of the 2 incretin receptors following their stimulation with native agonists in beta cells. While the GLP-1R is a rapidly internalizing receptor with increased propensity for β-arrestin 2 recruitment, endosomal localization and activity, and lysosomal degradation, the GIPR is associated with reduced coupling to G proteins and β-arrestin 2, as well as reduced internalization and endosomal activity, increased recycling, and an overall increase in beta cell signaling despite highly reduced levels of endogenous surface receptor expression. These characteristics suggest that GLP-1R and GIPR signaling from beta cells are differentially regulated, and might potentially engage distinct signal transduction and amplification mechanisms, highlighting the rationale for the development of dual agonists eliciting complementary beneficial effects from each receptor, as exemplified by the successful clinical development of the dual GLP-1R—GIPR agonist tirzepatide (11), a ligand which combines reduced internalization and β-arrestin 2 recruitment at the GLP-1R with GIPR stimulation (39).

Our study raises several conceptual issues: why is a receptor with reduced tendency for desensitization such as GIPR more easily exhausted in T2D conditions? We can speculate that the reduced level of expression of GIPR vs GLP-1R in beta cells under normal conditions might result in the selective preservation of GLP-1 responses in a context where expression of both receptors is compromised; alternatively, as our results point to a higher reliance on signal amplification mechanisms for the GIPR, it is possible that beta cell GIP responses are more dependent on conservation of downstream signaling mechanisms that might become dysfunctional in T2D. With regards to the apparent beneficial effects of both GIPR agonists and antagonists in controlling blood glucose levels, it is difficult to infer any direct answers from the present study as antagonist effects might be indirect, potentially involving weight loss or control of glucagon hypersecretion from alpha cells. We can only speculate that any direct effect on beta cells could conceivably be linked to the increased propensity for basal coupling of the GIPR, with antagonists possibly affecting the balance of free and bound effectors available for productive signal transduction. In the future, it would be interesting to test the effect of both GLP-1R and GIPR antagonists in our beta cell systems to further investigate this possibility.

The present study highlights profound differences in the behavior of both incretin receptors in beta cells. It is therefore likely that underlying regulatory mechanisms specific for each receptor exist. These might include unique sets of interacting proteins and lipids as well as specific receptor post-translational modifications that can potentially regulate the trafficking and signaling of each receptor individually. A thorough investigation of these processes is now paramount to design novel treatment strategies for T2D and obesity based on enhancing the individual signaling output of each receptor for maximal effect.

Acknowledgments

This work was supported by MRC grant number MR/R010676/1 to A.T. and B.J., and by UKRI COVID-19 Grant Extension Allocation (coA) to A.T. A.T. also acknowledges further support from the EFSD, Diabetes UK, Eli Lilly, the Commonwealth, and the Integrated Biological Imaging Network (IBIN). The authors thank Dr. Aida Martinez-Sanchez, Imperial College London, UK, for providing animal project license access and Dr. Kyle Sloop, Eli Lilly and Company, Indianapolis, Indiana, USA, for the *Gipr*$^{-/-}$ mice.

Disclosures

The authors have nothing to disclose.

Data Availability

Original data generated and analyzed during this study are included in this manuscript.

References

1. Seino Y, Fukushima M, Yabe D. GIP And GLP-1, the two incretin hormones: similarities and differences. *J Diabetes Investig*. 2010;1-(1-2):8-23.
2. Thorens B. Expression cloning of the pancreatic beta cell receptor for the gluco-incretin hormone glucagon-like peptide 1. *Proc Natl Acad Sci U S A*. 1992;89(18):8641-8645.
3. Volz A, Goke R, Lankat-Buttgereit B, Fehmann HC, Bode HP, Goke B. Molecular cloning, functional expression, and signal transduction of the GIP-receptor cloned from a human insulinoma. *FEBS Lett*. 1995;373(1):23-29.
4. Yamada Y, Hayami T, Nakamura K, *et al*. Human gastric inhibitory polypeptide receptor: cloning of the gene (GIPR) and cDNA. *Genomics*. 1995;29(3):773-776.
5. Nauck MA, Quast DR, Wefers J, Meier JJ. GLP-1 receptor agonists in the treatment of type 2 diabetes—state-of-the-art. *Mol Metab*. 2021;46:101102.
6. Tan Q, Akindehin SE, Orsso CE, *et al*. Recent advances in incretin-based pharmacotherapies for the treatment of obesity and diabetes. *Front Endocrinol (Lausanne)*. 2022;13:838410.
7. Boer GA, Keenan SN, Miotto PM, Holst JJ, Watt MJ. GIP Receptor deletion in mice confers resistance to high-fat diet-induced obesity via alterations in energy expenditure and adipose tissue lipid metabolism. *Am J Physiol Endocrinol Metab*. 2021;320(4):E835-E845.
8. Gasbjerg LS, Gabe MBN, Hartmann B, *et al*. Glucose-dependent insulinotropic polypeptide (GIP) receptor antagonists as anti-diabetic agents. *Peptides*. 2018;100:173-181.
9. Yang B, Gelfanov VM, El K, *et al*. Discovery of a potent GIPR peptide antagonist that is effective in rodent and human systems. *Mol Metab*. 2022;66:101638.
10. Campbell JE. Targeting the GIPR for obesity: to agonize or antagonize? Potential mechanisms. *Mol Metab*. 2021;46:101139.
11. Min T, Bain SC. The role of tirzepatide, dual GIP and GLP-1 receptor agonist, in the management of type 2 diabetes: the SURPASS clinical trials. *Diabetes Ther*. 2021;12(1):143-157.
12. Manchanda Y, Bitsi S, Kang Y, Jones B, Tomas A. Spatiotemporal control of GLP-1 receptor activity. *Curr Opin Endocr Metab Res*. 2021;16:19-27.
13. Jones B, Buenaventura T, Kanda N, *et al*. Targeting GLP-1 receptor trafficking to improve agonist efficacy. *Nat Commun*. 2018;9(1):1602.
14. Yabe D, Seino Y. Two incretin hormones GLP-1 and GIP: comparison of their actions in insulin secretion and beta cell preservation. *Prog Biophys Mol Biol*. 2011;107(2):248-256.

15. Younan SM, Rashed LA. Impairment of the insulinotropic effect of gastric inhibitory polypeptide (GIP) in obese and diabetic rats is related to the down-regulation of its pancreatic receptors. *Gen Physiol Biophys*. 2007;26(3):181-193.
16. Zhou J, Livak MF, Bernier M, *et al.* Ubiquitination is involved in glucose-mediated downregulation of GIP receptors in islets. *Am J Physiol Endocrinol Metab*. 2007;293(2):E538-E547.
17. Oduori OS, Murao N, Shimomura K, *et al.* Gs/Gq signaling switch in beta cells defines incretin effectiveness in diabetes. *J Clin Invest*. 2020;130(12):6639-6655.
18. Miki T, Minami K, Shinozaki H, *et al.* Distinct effects of glucose-dependent insulinotropic polypeptide and glucagon-like peptide-1 on insulin secretion and gut motility. *Diabetes*. 2005;54(4):1056-1063.
19. Aaboe K, Knop FK, Vilsboll T, *et al.* KATP Channel closure ameliorates the impaired insulinotropic effect of glucose-dependent insulinotropic polypeptide in patients with type 2 diabetes. *J Clin Endocrinol Metab*. 2009;94(2):603-608.
20. Naylor J, Suckow AT, Seth A, *et al.* Use of CRISPR/Cas9-engineered INS-1 pancreatic beta cells to define the pharmacology of dual GIPR/GLP-1R agonists. *Biochem J*. 2016;473(18):2881-2891.
21. Fang Z, Chen S, Pickford P, *et al.* The influence of peptide context on signaling and trafficking of glucagon-like peptide-1 receptor biased agonists. *ACS Pharmacol Transl Sci*. 2020;3(2):345-360.
22. Jaccard N, Griffin LD, Keser A, *et al.* Automated method for the rapid and precise estimation of adherent cell culture characteristics from phase contrast microscopy images. *Biotechnol Bioeng*. 2014;111(3):504-517.
23. Fang Z, Chen S, Manchanda Y, *et al.* Ligand-specific factors influencing GLP-1 receptor post-endocytic trafficking and degradation in pancreatic Beta cells. *Int J Mol Sci*. 2020;21(21):8404.
24. Buenaventura T, Bitsi S, Laughlin WE, *et al.* Agonist-induced membrane nanodomain clustering drives GLP-1 receptor responses in pancreatic beta cells. *PLoS Biol*. 2019;17(8):e3000097.
25. Morana O, Nieto-Garai JA, Bjorkholm P, *et al.* Identification of a new cholesterol-binding site within the IFN-gamma receptor that is required for signal transduction. *Adv Sci (Weinh)*. 2022;9(11):e2105170.
26. Pickford P, Lucey M, Fang Z, *et al.* Signalling, trafficking and glucoregulatory properties of glucagon-like peptide-1 receptor agonists exendin-4 and lixisenatide. *Br J Pharmacol*. 2020;177(17):3905-3923.
27. Rossow MJ, Sasaki JM, Digman MA, Gratton E. Raster image correlation spectroscopy in live cells. *Nat Protoc*. 2010;5(11):1761-1774.
28. Garcia E, Bernardino de la Serna J. Dissecting single-cell molecular spatiotemporal mobility and clustering at focal adhesions in polarised cells by fluorescence fluctuation spectroscopy methods. *Methods*. 2018;140-141:85-96.
29. Compte M, Harwood SL, Munoz IG, *et al.* A tumor-targeted trimeric 4-1BB-agonistic antibody induces potent anti-tumor immunity without systemic toxicity. *Nat Commun*. 2018;9(1):4809.
30. Muntean BS, Zucca S, MacMullen CM, *et al.* Interrogating the spatiotemporal landscape of neuromodulatory GPCR signaling by real-time imaging of cAMP in intact neurons and circuits. *Cell Rep*. 2018;22(1):255-268.
31. Klarenbeek JB, Goedhart J, Hink MA, Gadella TW, Jalink K. A mTurquoise-based cAMP sensor for both FLIM and ratiometric read-out has improved dynamic range. *PLoS One*. 2011;6(4):e19170.
32. Manchanda Y, Bitsi S, Chen S, *et al.* Data from: Enhanced endosomal signaling and desensitization of GLP-1R versus GIPR in pancreatic beta cells. figshare 2023. Deposited February 1, 2023. https://doi.org/10.6084/m9.figshare.21992441.v12023.
33. Jones BJ, Scopelliti R, Tomas A, Bloom SR, Hodson DJ, Broichhagen J. Potent prearranged positive allosteric modulators of the glucagon-like peptide-1 receptor. *ChemistryOpen*. 2017;6(4):501-505.
34. Samms RJ, Christe ME, Collins KA, *et al.* GIPR Agonism mediates weight-independent insulin sensitization by tirzepatide in obese mice. *J Clin Invest*. 2021;131(12):e146353.
35. DiGruccio MR, Mawla AM, Donaldson CJ, *et al.* Comprehensive alpha, beta and delta cell transcriptomes reveal that ghrelin selectively activates delta cells and promotes somatostatin release from pancreatic islets. *Mol Metab*. 2016;5(7):449-458.
36. Chandra M, Kendall AK, Jackson LP. Toward understanding the molecular role of SNX27/retromer in human health and disease. *Front Cell Dev Biol*. 2021;9:642378.
37. Jones B, McGlone ER, Fang Z, *et al.* Genetic and biased agonist-mediated reductions in beta-arrestin recruitment prolong cAMP signaling at glucagon family receptors. *J Biol Chem*. 2021;296:100133.
38. McGlone ER, Manchanda Y, Jones B, *et al.* Receptor activity-modifying protein 2 (RAMP2) alters glucagon receptor trafficking in hepatocytes with functional effects on receptor signalling. *Mol Metab*. 2021;53:101296.
39. Novikoff A, O'Brien SL, Bernecker M, *et al.* Spatiotemporal GLP-1 and GIP receptor signaling and trafficking/recycling dynamics induced by selected receptor mono- and dual-agonists. *Mol Metab*. 2021;49:101181.
40. Al-Sabah S, Al-Fulaij M, Shaaban G, *et al.* The GIP receptor displays higher basal activity than the GLP-1 receptor but does not recruit GRK2 or arrestin3 effectively. *PLoS One*. 2014;9(9):e106890.
41. van Gastel J, Hendrickx JO, Leysen H, *et al.* beta-Arrestin based receptor signaling paradigms: potential therapeutic targets for Complex age-related disorders. *Front Pharmacol*. 2018;9:1369.
42. Ferre S, Ciruela F, Dessauer CW, *et al.* G protein-coupled receptor-effector macromolecular membrane assemblies (GEMMAs). *Pharmacol Ther*. 2022;231:107977.
43. Marzook A, Chen S, Pickford P, *et al.* Evaluation of efficacy- versus affinity-driven agonism with biased GLP-1R ligands P5 and exendin-F1. *Biochem Pharmacol*. 2021;190:114656.